Evaluation of 1,2-diacyl-3-acetyl triacylglycerol production in *Yarrowia lipolytica*

Authors:

Qiang Yan[1,2] Tyler B. Jacobson[3,4,5], Zhou Ye[1], Yoel R. Cortés-Peña[6,7], Sarang S. Bhagwat[6,7], Susan Hubbard[1,2,], William T Cordell[1,2], Rebecca E. Oleniczak[1,2], Francesca V. Gambacorta[1,4], Julio Rivera Vazquez[3,4,5,8], Eric V. Shusta[1,9], Daniel Amador-Noguez[3,4,5,6.], Jeremy S. Guest[6,7], and Brian F. Pfleger[1,2,4,8,*]

Affiliations:

[1] Department of Chemical and Biological Engineering, University of Wisconsin-Madison, Madison, WI 53706, United States.

[2] DOE Center for Advanced Bioenergy and Bioproducts Innovation, University of Wisconsin-Madison, Madison, WI 53706, United States.

[3] Department of Bacteriology, University of Wisconsin-Madison, Madison, WI, USA.

[4] DOE Great Lakes Bioenergy Research Center, University of Wisconsin-Madison, Madison, Wisconsin, United States of America.

[5] DOE Center for Bioenergy Innovation, Oak Ridge National Laboratory, Oak Ridge, Tennessee, USA.

[6] DOE Center for Advanced Bioenergy and Bioproducts Innovation (CABBI), University of Illinois Urbana-Champaign, 1206 W. Gregory Drive, Urbana, IL 61801, USA.

[7] Department of Civil and Environmental Engineering, University of Illinois Urbana-Champaign, 3221 Newmark Civil Engineering Laboratory, 205 N. Mathews Avenue, Urbana, IL 61801, USA.

[8] Microbiology Doctoral Training Program, University of Wisconsin-Madison, Madison, WI 53706, United States.

[9] Department of Neurological Surgery, University of Wisconsin–Madison, 1415 Engineering Drive, Madison, WI, 53706, USA.

* Corresponding author. 3629 Engineering Hall, 1415 Engineering Drive, Madison, WI 53706, United States. Phone: +1 608 890 1940. Fax: +1 608 262-5434. E-mail address: brian.pfleger@wisc.edu

Abstract

Plants produce many high-value oleochemical molecules. While oil-crop agriculture is performed at industrial scales, suitable land is not available to meet global oleochemical demand. Worse, establishing new oil-crop farms often comes with the environmental cost of tropical deforestation. The field of metabolic engineering offers tools to transplant oleochemical metabolism into tractable hosts while simultaneously providing access to molecules produced by non-agricultural plants. Here, we evaluate strategies for rewiring metabolism in the oleaginous yeast *Yarrowia lipolytica* to synthesize a foreign lipid, 3-acetyl-1,2-diacyl-sn-glycerol (acTAG). Oils made up of acTAG have a reduced viscosity and melting point relative to traditional triacylglycerol oils making them attractive as low-grade diesels, lubricants, and emulsifiers. This manuscript describes a metabolic engineering study that established acTAG production at g/L scale, exploration of the impact of lipid bodies on acTAG titer, and a techno-economic analysis that establishes the performance benchmarks required for microbial acTAG production to be economically feasible.

Introduction

The chemical industry is seeking green alternatives to conventional petrochemical products in an effort to address global climate change and establish a sustainable economy. Biofuels, targeted for combustion in personal transportation, heavy transportation, and aviation sectors, have received the most attention due to the enormous volumes consumed each year and the corresponding size of their financial and environmental impact[1–3]. A smaller fraction of each barrel of oil is used as the source of petrochemicals including molecules used as lubricants and emulsifiers. Sustainable sources of these oleochemical products are also needed. Plant oils are an alternative source of biodiesel and oleochemicals, but plant-based production is linked with tropical deforestation and is limited in scale[4]. Another promising alternative is the microbial synthesis of oils and oleochemicals. Oleaginous microbes, such as *Yarrowia lipolytica*, produce lipid bodies to store oils, typically in the form of long-chain triacyl glycerol (lcTAG) analogous to many oil crops. The high rate of fatty acid biosynthesis and lipid storage native to oleaginous microbes has been exploited to produce lcTAG[5,6] and other non-native products[7–9]. One potentially interesting lipid, 3-acetyl-1,2-diacyl-*sn*-glycerol (acTAG) contains long-chain fatty acids linked to the *sn*-1 and *sn*-2 hydroxyls of glycerol, but an acetic acid at the *sn*-3 position instead of the larger fatty acids in lcTAGs (**Supplementary Fig. 1**). The shorter acetate moiety leads acTAG to have lower kinematic viscosity, lower melting point, and reduced calorific values[10–12] relative to lcTAG molecules (**Supplementary Table 1**). These properties cast acTAGs in many promising industrial applications such as low-speed diesel fuels, emulsifiers, food coatings, and plasticizers[13]. In addition, acTAGs have been used in therapeutic applications such as “functional foods” and pharmaceuticals for asthma[14–16]. In this study, we set two goals: to develop a *Y. lipolytica* strain capable of producing acTAG at g/L titer and to evaluate the feasibility of microbial acTAG production.

In nature, acTAG are found in plants of the family *Celastraceae.* For example, the developing seed oil of *Euonymus alatus* (burning bush) is comprised of 98% acTAGs[17]. In *Euonymus* species, acTAG are synthesized by acetylation of the *sn*-3 hydroxyl group of diacylglycerol (DAG), a reaction catalyzed by *sn*-1,2-diacylglycerol:acyl-CoA acyltransferases. The first gene encoding a *sn*-1,2-diacylglycerol:acyl-CoA acyltransferase was identified from *E. alatus* (*^{EUOal}DGAT1*) and belongs to the DGAT1 gene family. Purified ^{EUOal}DGAT1 was shown to have *in vitro* acTAG synthesis activity by incubating [^{14}C]acetyl-CoA with endogenous DAG and ^{EUOal}DGAT1 from microsomal fraction of *S. cerevisiae* expressing ^{EUOal}DGAT1 produced [^{14}C]acetyl-TAG, whereas control strain expressing no enzyme did not produce the product[17]. However, heterologous expression of ^{EUOal}DGAT1 in *S. cerevisiae* failed to produce acTAG *in vivo*, but rather enhanced lcTAG titer. In a later study, Durrett et al., investigated low-abundance transcripts in *Euonymus* and identified a highly selective diacylglycerol acetyltransferase ^{EUOal}DAcT from *Euonymus alatus*. ^{EUOal}DAcT was distantly related to common acyl-transferases in the family of membrane-bound *O*-acyltransferase (MBOAT) (http://pfam.xfam.org/family/MBOAT)[11]. Overexpressing ^{EUOal}DAcT in *S. cerevisiae* led to acTAG production but did not significantly increase lcTAG titer. Further *in vitro* experimental evidence indicated that ^{EUOal}DAcT has a preference towards acetyl-CoA and suggested that ^{EUOal}DAcT has little activity towards acyl-CoAs longer than eight carbons[18]. In the same study, the authors also found that ^{EUOal}DAcT preferentially acetylated unsaturated DAG molecules over saturated DAG molecules. ^{EUOal}DAcT embeds in the phospholipid bilayer of endoplasmic reticulum (ER), where DAG, one of its substrates, is synthesized in lipid metabolism. Experimental evidence demonstrating the source (cytosol or ER lumen) of the acetyl-CoA is lacking. The structure of ^{EUOal}DAcT has yet to be solved but a topology model supports its classification as a membrane protein. The model suggested that ^{EUOal}DAcT has four transmembrane domains (TMDs), with both the N- and C-termini oriented toward the lumen of the ER, and a large cytoplasmic loop between the first and second

transmembrane domains[19]. Oleaginous yeasts, plants and other eukaryotes are the logical hosts for production of acTAGs because of the transmembrane constraint of DAcT and the presence of lipid bodies as a means of acTAG storage.

Lipid bodies are dynamic organelles used for lipid and energy homeostasis in cells. They consist of a core of neutral lipids encircled by a phospholipid monolayer that is decorated with integral and peripheral proteins[20]. Lipid bodies provide an isolated hydrophobic environment away from the cytosol and serve as a product sink for sequestering neutral lipids. Generally, lipid body formation follows three steps: first, neutral lipids are synthesized and accumulate within the ER phospholipid bilayer, then a lens forms as the oil phase coalesces, and finally the bilayer deforms and a nascent lipid body buds into the cytoplasm[21]. However, precisely how lipid body assembly is triggered remains unclear. For instance, small molecules such as lcTAG or sterol esters can trigger lipid body formation, but it remains unclear whether other oleochemical products, such as acTAG, fatty alcohols and alkanes, can also have this effect. It is also unclear whether neutral lipid lenses form randomly throughout the ER or whether there are preferential sites for their formation. Critically, how proteins on the ER membrane and/or lipid body surface promote LB budding is also unsolved[22]. Recent literature suggests that the presence of a lipid body boosts hydrophobic compound production[23–25]. In this study, we found a strong correlation between the presence of lipid bodies and acTAG titer; motivating further basic science studies to enable future metabolic engineering projects.

The production of acTAG has been improved via metabolic engineering in several hosts including oilseed plants and yeast. *Camelina* and soybean were engineered to express ^{EUOal}DAcT and to produce acTAG[12]. RNAi targeting DGAT1 in *Camelina* suppressed endogenous lcTAG production, and increased acTAG synthesis[12], and an engineered *Camelina sativa* line achieved

123 acTAG production representing 70% of total seed oil and 26% (g/g) of the seed dry cell weight.
124 The *sn*-1 and *sn*-2 acyl chain-length composition of acTAG was further tailored by expressing a
125 medium-chain acyl-CoA thioesterase FatB in *C. sativa*[26]. The transgenic *C. sativa* line produced
126 acTAGs representing 77 mol% of total seed oils and 37% (g/g) of the seed dry cell weight. When
127 ^{EUOal}DAcT was expressed in a wild-type *Saccharomyces cerevisiae* SCY62 or an engineered 4KO
128 strain (GLBRC40, *ΔDGA1 ΔLRO1 ΔARE1 ΔARE2)*, acTAG production reached 2.4 mg/g DCW
129 and 3 mg/g DCW, respectively[27]. These titers served as a proof of concept but are insufficient for
130 commercial production. While *S. cerevisiae* has been engineered to produce oleochemicals at
131 high levels[28,29], oleaginous yeasts may offer a better starting point for acTAG production. When
132 *Euonymus europaeus* ^{EUOeu}DAcT was expressed in *Y. lipoltytica* Po1d and JMY1877, an
133 engineered derivative (Po1d, *ΔDGA1 ΔLRO1 ΔARE1 ΔDGA2*), low levels of acTAG (30.6 mg/g
134 DCW and 3.1 mg/g DCW) were produced, respectively[30]. This study established the feasibility of
135 producing acTAG in *Y. lipolytica* and motivated the current study to improve strain performance
136 via metabolic engineering.

137

138 In this work, we employ a combination of metabolic engineering strategies to explore acTAG
139 production in *Y. lipolytica* (**Fig. 1**). We first create a suite of strains to eliminate lcTAG synthesis
140 and lipid degradation in an effort to maximize flux to DAG, the acTAG precursor. We establish
141 acTAG production in these strains by heterologously expressing the best acTAG synthase
142 identified from a bioprospecting study. The family of strains establish a strong link between lipid
143 body formation and acTAG titer. Next, we used a family of promoters to titrate DGA1 and DGA2
144 activity and obtain strains where lcTAG titer is substantially reduced yet lipid body formation is
145 maintained. Titrating DGA1 and DGA2 using lower strength promoters increases acTAG by 1.4-
146 to 5-fold. We combined our engineering efforts into two production strains, one that maximizes
147 acTAG production titer but contains large amounts of lcTAG and another that maximizes the ratio

of acTAG:lcTAG (minimizing purification needs). A production strain expressing a xylose catabolic pathway, generates 4 g/L acTAG when grown on sugarcane juice and 2.5 g/L acTAG when grown on oilcane hydrolysate. The same strains when cultured in fed batch with laboratory media achieves 12 g/L acTAG titer. We describe a new techno-economic model of acTAG production and evaluate the impact of bioprocess parameters (e.g., yield, titer, selectivity, productivity) on minimum selling price (MSP). The analysis suggests that strains achieving acTAG production at 85% theoretical yield, 90 g/L titer, 75% acTAG selectivity, and 1.0 g/L/h productivity would be feasible for commercialization of commercial emulsifiers. Together, this research demonstrates novel strategies for improving production of non-native neutral lipids in *Y. lipolytica* and metabolic engineering targets for industrialization.

Results and Discussion

*EUOal*DAcT can be functionally expressed in *Yarrowia lipolytica*

The key enzymatic activity required for synthesis of acTAG is the transesterification of acetyl-CoA with a DAG, a reaction catalyzed by a unique member of the MBOAT superfamily of proteins[11]. We selected two previously characterized acTAG synthases (e.g. *EUOal*DAcT and *EUOal*DGAT1)[11,17] from *Euonymus alatus* to evaluate their function in wild-type *Yarrowia lipolytica* PO1f. The expression cassette TEFp-[*EUOal*DAcT/*EUOal*DGAT1]-CYCt-tub1p-HPH was randomly integrated into the PO1f chromosome. Cells were cultured in YSC medium for 96 hrs. Lipids were extracted and examined using ESI-MS. We found that the PO1f strain expressing *EUOal*DAcT accumulated acTAGs, but the PO1f strain expressing *EUOal*DGAT1 did not, equivalent to a sample from a strain harboring an empty vector. The mass spectrum of the *EUOal*DAcT sample contained two ions (m/z = 685.43 and 663.45) that were consistent with the [M+Na]+ and [M+H]+ adducts of acTAG containing two oleic acid chains (i.e. 18:1, 18:1, 2:0), respectively (**Supplementary Fig. 2)**. These results are consistent with prior studies that demonstrated *EUOal*DAcT has acetylating activity on unsaturated DAG substrates[18] and reported high abundance

of the 18:1, 18:1-DAG species in *Y. lipolytica*[31]. These results confirmed the ability of *Y. lipolytica* to produce acTAG and motivated further metabolic engineering efforts.

Combinatorial metabolic engineering strategies to enhance acTAG production

To maximize flux to a desired product, metabolic engineers often genetically modify microbes to block competing pathways, to deregulate pathway activity, to overexpress rate-limiting enzymes, and to address product toxicity. In this study, we hypothesized that acTAG titer could be enhanced by implementing three metabolic engineering strategies including 1) removing endogenous TAG synthesis and TAG degradation, i.e., competing pathways, 2) identifying highly active acTAG synthases to pull flux into lipid synthesis, and 3) engineering lipid body formation to minimize the physiological impact of acTAG (**Fig. 1**). We constructed six base strains, designated QY01 to QY06 by iteratively deleting key enzymes in competing pathways. Specifically, we started with wild-type PO1f and deleted three lcTAG synthases (DGA1, DGA2 and LRO1), two lipases (TGL3 and TGL4), and a glycerol-3-phosphate dehydrogenase GUT2 (**Supplementary Fig. 3**). The deletion of GUT2 helps push carbon flux into the TAG synthesis pathway[32]. The lipid profile of each engineered strain was quantified from samples of cells grown at 30°C for 120 hrs in YSC media containing 80 g/L glucose. Total lipid content was characterized by GC-FID mediated fatty acid methyl ester (FAME) analysis of lipid samples derivatized by transesterification. Compared to the total FAME in PO1f strain, deletion of two lipases (TGL3 and TGL4 in QY01 and QY02) did not alter overall FAME titer. Deletion of DGA1 (TAG synthase) in QY03 significantly dropped total FAME titer to 10% of the base PO1f. Deletion of LRO1 in QY04 did not affect FAME titer relative to QY03. As expected, deletion of GUT2, in strain QY05 increased total FAME titer 3-fold relative to QY04 (**Fig. 2A**). Deletion of DGA2 in strain QY06 reduced lipid titers by 90% relative to the base strain PO1f (20% relative to its parent QY05). These observations confirm that native TAG content could be substantially

197 reduced with the residual FAME observed in samples of QY06 likely coming from essential
198 phospholipids.

199

200 To confirm the loss of lcTAG, we analyzed lipid body formation via staining with Nile red, a
201 lipophilic fluorescent dye. Strain QY06 grew to a lower optical density than the base strain PO1f
202 **(Fig. 2B)** and generated a substantially reduced Nile red signal over time (**Fig. 2C**). Samples
203 taken at 120 hrs were fixed for analysis by fluorescence microscopy. Images of strain PO1f
204 showed brightly fluorescent spots within the cell boundary, consistent with the expected presence
205 of lipid bodies. In contrast, images of QY06 cells were dramatically less fluorescent and did not
206 contain noticeable subcellular aggregates; indicating that cells failed to form lipid bodies (**Fig.**
207 **2D**).

208 Experiments with strain QY06 were complicated by its slow growth rate. Later, we discovered
209 that the strain recovered from freezer stocks poorly and had a lower DNA transformation
210 efficiency ($<10^2$ CFU/μg DNA) relative to its predecessors. Therefore, to improve its growth, we
211 adaptively evolved strain QY06 in YPD liquid media for ~60 days or ~300 generations
212 (**Supplementary method 1)**. The endpoint evolved strain, named QY06R, grew faster (doubling
213 time 4.5 hrs compared to the QY06 strain of 6 hrs) (**Supplementary Fig. 4**) and was more
214 efficiently transformed (~10^4 CFU/ μg DNA) using pY5 empty vector. The genome sequence of
215 strain QY06R contained 39 mutations relative to the genome of QY06 (**Supplementary data 1**).
216 None of the 39 mutations implied a clear rationale for the growth improvement.

217 **acTAG titer is influenced by the presence of lipid bodies**

218 We conducted a bioprospecting study (**Supplementary Method 2, Supplementary Fig. 5-8**) to
219 identify highly active acTAG synthases but failed to identify an enzyme with activity superior to
220 the ^{EUOal}DAcT variant described in the first section. Therefore, we transformed the pY5-*URA3*-

221 ^{EUOal}*DAcT-LEU2* expression plasmid into each of the *Y. lipolytica* strains PO1f, QY01-QY05 and
222 QY06R and quantified the relative amounts of acTAG and lcTAG from cultures of each strain.
223 Lipid titers were quantified by HPLC-MS and lipid body formation was qualitatively assessed by
224 confocal microscopy. A representative membrane lipid Phosphatidylglycerol (PG, 16:0,16:0) was
225 used as a proxy for cellular biomass, and peak area ratios of TAG to PG were used to approximate
226 lipid abundance per dry cell weight. A chemically synthesized acTAG standard (17:0, 17:0, 2:0)
227 and a commercially available lcTAG standard (17:0, 17:0, 17:0) eluted at 15.6 min and 19.0 min,
228 and resulted in detectable $[M+NH_4]+$ adducts with the expected m/z 565.58 and 866.82 in
229 positive ion mode (**Fig. 3A**). No ions corresponding to acTAG were identified in samples of
230 QY06R strain harboring the empty pY5 plasmid (**Fig. 3A**). Strains expressing ^{EUOal}*DAcT*
231 produced three major acTAG species (m/z 624.52, 652.55, and 680.58, corresponding to
232 $[M+NH_4]+$ adducts of acTAGs (16:1,16:1,2:0, 16:1,18:1,2:0 and 18:1,18:1,2:0) at elution time
233 (13.4, 14.8, and 15.9 min), respectively (representative chromatograms for samples from QY02
234 and QY06R are shown in **Fig. 3A** and the rest are available as **Supplementary Fig. 9**,
235 corresponding acTAG mass spectra are available as **Supplementary Fig.10**). The amounts of
236 acTAG and lcTAG varied significantly across the strains with a strong proportionality between
237 acTAG and lcTAG abundance (**Fig. 3B**, **3C**, and **Supplementary Fig. 11**). Among engineered
238 strains, QY02 expressing ^{EUOal}DAcT produced the highest amount of acTAG and lcTAG (**Fig.**
239 **3A**, **3B** and **3C**), and formed clear lipid bodies (**Fig. 3D**). QY06R expressing ^{EUOal}DAcT
240 produced almost exclusively (97%) acTAG (**Fig. 3A**, **3B**, and **3C**) at a reduced titer without any
241 visible lipid bodies (**Fig. 3D**). Rather, the nile red stain was diffuse across the entire cell. Our data
242 suggests that lipid bodies are beneficial to the production of acTAGs and replacement of lcTAG
243 synthases with acTAG synthases does not restore lipid body formation.

244 **Engineering lipid body to enhance acTAG titer**

Given the strong positive correlation of acTAG titer and lipid body formation, we pursued strategies to restore lipid body formation while minimizing flux to lcTAG. Lipid bodies and lcTAG were observed in all strains except QY06 and QY06R, at which point both DGA1 and DGA2 were deleted. Gajdoš et al., found both enzymes are capable of restoring lipid body formation and synthesizing lcTAG in an engineered strain (Po1d, *ΔDGA1 ΔLRO1 ΔARE1 ΔDGA2*)[33]. Interestingly, expressing DGA1 generates small but numerous LBs while expressing DGA2 forms large LBs. DGA2 belongs to DGAT1 family protein that localizes in ER bilayer[34], whereas ^{Yl}DGA1 belongs to DGAT2 family protein that can be accommodated in both the ER bilayer and lipid body monolayer[35]. The mechanism of lipid body formation is not well understood, but in general is thought to proceed by budding from the ER membrane after neutral lipids are locally concentrated. The molecular signals for budding could include structural protein components, molecule concentrations, and/or biophysical traits within the membrane. Given our goal of packaging acTAG in lipid bodies, we were curious if lipid body assembly could be restored by expression of catalytically inactive TAG synthase (E.C. 2.3.1.20), thereby testing the hypothesis of a structural, non-catalytic role of DGA2 in lipid body formation. For this experiment, we integrated the ^{EUOal}DAcT expression cassette into strain QY06R, generating QY07 (QY06R, *IntC2:: URA3-*^{EUOal}*DAcT-LEU2*). QY07 produced acTAG but did not produce lcTAG or form lipid bodies (**Fig. 4A**, **4B and 4C**). We created an inactive variant of DGA2 by making point mutations to catalytic residues (H453A E454A), as shown previously[36] and **Supplementary Fig. 12**, and cloned the ORF into a pY5-based expression plasmid. After 120 hr of growth, extracts of *Y. lipolytica* QY07 expressing dDGA2 contained no detectable lcTAG and microscope images showed no lipid body assembly. In contrast, QY07 cells expressing the active DGA2 in the same plasmid accumulated lcTAG and triggered lipid body assembly. All QY07 strains produced acTAG and interestingly, QY07 expressing dDGA2 produced 2.1-fold (P=0.04) more acTAG than QY07 harboring an empty vector (**Fig. 4A**, **4B** and **4C**). We attempted an

analogous experiment with DGA1, using sequence alignments to predict active site residues, but this variant kept its TAG synthesis activity (**Supplementary Fig. 13**). While we cannot conclude that DGA1/2 activity is required for lipid body formation, our data suggests that acTAG do not functionally replace the presence of lcTAG in lipid body formation.

If lcTAG synthesis was necessary for lipid body formation, we were curious to discover if we could minimize DGA1/DGA2 activity and maximize the ratio of acTAG:lcTAG. We designed vectors to titrate expression of DGA1 or DGA2 using six promoters of varied strength (e.g., TEFp > FBAp > GPDp > GPATp > XPR2p > YAT1p)[37]. Cultures of *Y. lipolytica* QY07 harboring one of the pY5NAT-'promoter'-DGA1/DGA2 plasmids were grown for 120 hrs and their lipid content was assayed by LC-MS and confocal microscopy (**Fig. 4**). In general, DGA1 expression led to 2-9 times more lcTAG (**Fig. 4A** and **4D**), and 1.5-4 times more acTAG accumulation than the corresponding DGA2 expressing strains (**Fig. 4B** and **4E**). The trend of lipid content under control of different strength promoters is generally consistent between DGA1 or DGA2 expression. Titrating DGA1 or DGA2 expression using lower strength promoter GPATp increased lcTAG and acTAG production and achieved a higher acTAG to lcTAG ratio. Expressing DGA1 or DGA2 using higher strength promoter continued to increase lcTAG production but acTAG titer reached a plateau leading to reduced acTAG:lcTAG ratios. We used confocal microscopic imaging techniques to quantify an average fluorescence area per cells to estimate a mean lipid body size. Cells expressing DGA1 under control of TEFp, FBAp and GPDp had a lipid body size 1.7-, 2.2- and 1.4-fold larger than cells expressing DGA2, respectively (**Fig. 4C** and **4F**, **Supplementary Table 2** and **Supplementary Fig. 14**). To this end, our data suggest that DGA1 has a stronger effect than DGA2 for promoting LB formation and enhancing acTAG titers.

Combining beneficial mutations in production strains

Our exploratory experiments suggested two strategies for maximizing acTAG production 1.) maximize total acTAG titer and purify it away from other lipids, and 2.) minimize purification needs by designing strains to produce the highest ratio of acTAG:lcTAG. To test each strategy, we consolidated beneficial genetic changes to create production strains. First, starting with *Y. lipolytica* QY02, which accumulated the highest acTAG titer (with plasmid based ^{EUOal}*DAcT* expression) and substantial lcTAG in lipid bodies (**Fig. 3**), we created two engineered strains. In the first, we integrated a ^{EUOal}DAcT expression cassette into the QY02 chromosome generating strain QY08 (QY02, *IntC2::URA3-*^{EUOal}*DAcT-LEU2*). Second, we deleted GUT2 from QY08, generating strain QY09 (QY08, *ΔGUT2*) to determine if the deletion enhanced acTAG titer as it did in transitioning from strain QY04 to QY05. *Y. lipolytica* QY09 increased acTAG titer 2- and 2.4-fold relative to QY08 and QY02 harboring pY5NAT-*URA3-*^{EUOal}*DAcT-LEU2* plasmid, respectively (**Fig. 5A** and **5B**). Second, starting with *Y. lipolytica* QY07, which produces acTAG but not lipid bodies, we created six strains, named QY10 – QY15, by titrating DGA1 or DGA2 expression with weaker promoters (GPATp, YAT1p or XPR2p). Each engineered strain improved acTAG titer between 1.4- to 5.0-fold relative to the base QY07 strain (**Fig. 5C**). Strain QY10 produced the most lipid, but only 6% was acTAG. Strain QY14 produced the highest percentage (75%) acTAG, but with only a 3.0-fold increase over QY07. Of the two strategies, *Y. lipolytica* QY09 produced substantially more acTAG, achieving the highest titer with ~50% selectivity.

To benchmark acTAG production, we performed a discontinuous fed-batch in a stirred-tank bioreactor by feeding pulses of glucose media after cells reached high cell density. During the fed-batch fermentation experiment, 100 g/L total glucose and 10 g/L ammonium sulfate were bolus-fed to the media at 72 hrs and fermentation was terminated at 192 hrs when fed glucose was depleted. At 192 hrs, cells consumed total 180 g/L glucose (**Fig. 6A**), produced ~48 g/L dry cell

weight (**Fig. 6B**) and 12 g/L acTAG (**Fig. 6C**). This experiment generated the highest reported acTAG titer to date.

Production of acTAG from plant feedstock

Sustainable production of low-cost transportation fuels and lubricants will require the use of low-cost renewable feedstocks. Therefore, we investigated acTAG production from agricultural feedstocks, sugarcane juice, oilcane hydrolysate[38], and switchgrass hydrolysate[39] produced by the Center for Advanced Bioenergy and Bioproducts Innovation. Here, *Y. lipolytica* QY07 and QY09 were cultured in 90% (v/v) sugarcane juice or 50% (v/v) switchgrass hydrolysate with 0.1 M phosphate buffer for 120 hrs. The feedstock compositions are listed in **Supplementary Table 3**. Total lipid titers were quantified by measuring derivatized FAME using GC-FID. We estimated the acTAG titer based on the fraction of total lipid (50 and 97%) made by QY09 and QY07 determined by selected ion abundance using HPLC-MS, where cells were grown in defined media (**Fig. 5A, 5B** and **5C**). After 120 hrs, QY07 strain consumed 27 g/L glucose and 23 g/L fructose in sugarcane juice, produced 15.6 g/L dry cell weight and 1.1 g/L acTAG, and QY09 strain consumed 27 g/L glucose and 23 g/L fructose in sugarcane juice, produced 15.5 g/L dry cell weight and 4.0 g/L acTAG (**Fig. 5D**). To enhance xylose utilization from hydrolysates, we constructed strain QY16 by integrating genes encoding a xylitol dehydrogenase, a xylose reductase and a xylulose kinase into the IntC3 loci of QY09 chromosome[40]. QY16 could grow on xylose as the sole carbon source (**Supplementary Fig. 15**). To test acTAG production from hydrolysate, QY09 and QY16 strains were grown in 50% (v/v) switchgrass hydrolysate or 50% (v/v) oilcane hydrolysate for 120 hrs. At 120 hrs, QY09 strain consumed 30 g/L xylose and 45 g/L glucose from oilcane hydrolysate, produced 1.6 g/L acTAG and 19.2 g/L DCW. At 120hrs, QY16 strain consumed 30 g/L xylose and 45 g/L glucose from oilcane hydrolysate, produced 2.5 g/L acTAG and 24.1 g/L DCW. (**Fig. 5E**). However, both strains grew poorly on 50% switchgrass hydrolysate, barely consumed any sugars and produced marginal amount of acTAG.

To this end, we corroborated that our engineered strains can produce acTAG over 1 g/L from renewable plant biomass feedstocks.

Techno-economic analysis

To assist in evaluating the feasibility of our metabolic engineering strategies, we constructed a techno-economic model of acTAG production in BioSTEAM[41,42]. The minimum selling price (MSP) of acTAG was evaluated across the yield, titer, selectivity, and productivity landscape for an oilcane biorefinery fermenting oilcane juice (OJ), and another fermenting both the oilcane juice and bagasse hydrolysate (OJH) (**Fig.7**). Overall, both configurations benefit more from improvements to yield than improvements to titer. Because the lipids and cell mass are mechanically separated from water, there was no need for distillation operations that are capital and utility intensive under low product titers. Discontinuities in the MSP slope across the titer and yield landscape are due to agile design requirements whereby a multi-effect evaporator was employed when a higher sugar concentration is required to achieve the specified titer while dilution water is used when a lower sugar concentration is required. Increasing the productivity decreases the MSP by lowering the number of fermentation reactors to achieve a given titer under the assumption that each fermenter volume can be maximally 3,785 m^3 (**Supplementary Method 3**). Lastly, increasing the selectivity decreases the MSP of acTAG when the MSP is above the price of biodiesel ($1,262 /MT). Conversely, if the MSP is above the price of biodiesel, increasing the selectivity further increases the MSP of acTAG.

Assuming a baseline fermentation performance based on the experiments conducted in this study (34% theoretical yield, 12 g/L titer, 50% acTAG selectivity, and 0.0625 g/L/h productivity), the OJ and OJH oilcane biorefineries would result in an MSP of $3,163 and $4,466 /ton (**Fig. 7A** and **7B**), respectively, which are higher than the market price range of acTAG both as a food grade emulsifier ($1,633–2,268 /ton)[43] and as a drop-in replacement for diesel #4 ($145–225 /ton)[44].

Although fermentation-derived acTAG would be economically infeasible under the current state of fermentation technologies, fermentative lcTAG production has been shown reach a performance as high as 57% theoretical yield, 85 g/L lcTAG, and productivity of 0.73 g/L/h[45]. Under a potentially feasible and industrially relevant fermentation performance target (55% theoretical yield, 30 g/L titer, 75 % acTAG selectivity, 0.7 g/L/h productivity), the OJ and OJH configurations would result in an MSP of $1,075 and $1,582 /ton, respectively (**Fig. 7A**), which is well below the market price range as a food emulsifier but above the market price range of diesel #4. Regardless of biorefinery performance, assuming that the price of oilcane is the same as sugarcane, the feedstock alone would contribute a production cost ($541 /ton acTAG), which is larger than the market price of diesel #4. Processing oilcane to produce acTAG may become profitable as a food emulsifier but is unlikely to be profitable as a drop-in replacement for diesel #4 given historical price data. In conclusion, with further research and development on the fermentation yield, productivity, and selectivity, fermentation-derived acTAG may serve as a market-competitive emulsifier that can increase the profitability of an oilcane biorefinery and drive the production of sustainable biodiesel.

Methods

Strains, plasmids, oligonucleotides, and reagents

E. coli DH5α was used as cloning host for plasmid construction. All *E. coli* and *Yarrowia lipolytica* strains were listed in **Supplementary data 2**. If not specified, *E. coli* was cultured in LB medium supplemented with required antibiotics (100 mg/L carbenicillin, 50 mg/L kanamycin, or 30 mg/L chloramphenicol) at 37°C and 250 r.p.m. *Y. lipolytica* PO1f (ATCC MYA-2613, MatA, leu2-270, ura3-302, xpr2-322, axp-2) was used as the parental strain[46]. QY04 and QY06R strains were used as hosts in bioprospecting experiments. QY09 strain was used in fed-batch fermentation experiments. QY16 strain was used in hydrolysate conversion experiments.

All plasmids used in the study are summarized in **Supplementary data 2**. Plasmid maps are available as **Supplementary data 3**. Oligonucleotide primers used in the study were annotated in the plasmid maps provided as **Supplementary data 3**. Genes encoding acTAG synthase homologs were designed and synthesized by the Joint Genome Institute (JGI). DNA encoding DGA2, dDGA2 (DGA2 H453A E454A), DGA1 and dDGA1 (DGA1 K377A R379A K379A E383A E387A E401A) were synthesized by IDT. Episomal plasmids pY5[47] or pY5NAT were used as shuttle vectors for cloning genes in *E. coli* and for expressing in *Y. lipolytica*. All plasmids were constructed by Gibson assembly cloning kits (New England Biolabs) or restriction enzyme digestion/ligation method[48]. All cloned sequences and gene deletions were confirmed by colony PCR and Sanger sequencing performed by Functional Biosciences (Madison, WI).

"YPD" medium (10 g/L yeast extract, 20 g/L peptone and 20 g/L glucose) was used for regular culture of yeast strains. "YPD+Nat/HygB" containing 300 mg/L nourseothricin sulfate or 300 mg/L hygromycin B were used for selection of transformants with resistance gene cassettes. "YSC-LEU/-URA" medium, containing 20 g/L glucose, 1.7 g/L yeast nitrogen base without amino acids and ammonium, 5 g/L ammonia sulfate, and 0.77 g/L complete supplement mixture without uracil/leucine (CSM-URA/-LEU, MP), was used for selection of transformers auxotrophic to uracil/leucine. Yeast cells were cultured at 30°C and 250 r.p.m. in liquid media. Cell density (OD_{600}) was measured by a spectrophotometer (ThermoScientific). All chemicals and substrates were purchased from Sigma-Aldrich unless otherwise indicated.

Strain construction

In the functional characterization experiment, expression cassette TEFp-[^{EUOal}DAcT/^{EUOal}DGAT1]-CYCt-tub1p-HPH was randomly integrated into the PO1f chromosome[46]. *Y. lipolytica* base strains QY01 through QY09 were constructed by sequentially deleting genes from strain PO1f. TGL3 and TGL4 deletion was performed by a markerless homologous recombineering-based method[49] yielding strains QY01 and QY02. To facilitate a

CRISPR/Cas9-based genome engineering approach[50], a *TEF1p-cas9-TEFt* cassette was integrated at the *IntB* loci of the QY02 chromosome. Deletions of DGA1, LRO1, GUT2, and DGA2 in *Y. lipolytica* QY02 were subsequently made by a CRISPR/Cas9 method, yielding strains QY03 - QY06, respectively. To select for specific guide RNAs, all potential gRNAs for a given gene were compared with all potential off-targets in the entire *Y. lipolytica* CLIB122 genome sequence using the online tool "CHOPCHOP"[51] (http://chopchop.cbu.uib.no/). The initial QY06 strain grew very slowly, so it was serially passaged in YPD liquid media for 30 days (~300 generations) and an evolved strain, QY06R, was isolated from a single colony. To evaluate acTAG production, strains (PO1f, QY01 to QY05, and QY06R) were transformed with pY5-TEFp-*^{EUOal}DAcT*-Lip2t. Strains QY07 and QY08 were constructed by the CRISPR/Cas9 method to integrate the expression cassette *LEU2-^{EUOal}DAcT-URA3* at the *IntC2* loci in the chromosome of QY06R and QY02, respectively. Strain QY09 was constructed by knocking out *GUT2* in QY08. Strains used for evaluation of DGA1 and DGA2 function were constructed by transforming pY5NAT-'TEFp'-'*DGA1'* or pY5NAT-'TEFp'-'*DGA2'* in strain QY07.

To vary the expression levels of DGA1 and DGA2, the promoters of GPAT, GDP, FBA, XPR2 and YAT1 were amplified from PO1f genomic DNA and cloned upstream of each ORF. Strains QY10 - QY15 were constructed by integrating a DGA1 or DGA2 expression cassette at IntE3 loci of QY07 chromosome. To enable xylose catabolism, strain QY16 was constructed by integrating a xylitol dehydrogenase (YALI1_E15452g), a xylose reductase (YALI1_D09870g) and a xylulose kinase (YALI0F10923) at IntC3 loci of the QY09 chromosome.

Y. lipolytica cultures for acTAG production

A single colony of *Y. lipolytica* was inoculated into 5 mL of defined liquid medium (0.77 g/L CSM or CSM-LEU or CSM-URA-LEU, 1.7 g/L yeast nitrogen base without amino acids and ammonium sulfate, 10 g/L ammonium sulfate, 80 g/L glucose, 100 mM phosphate buffer and

antibiotics as needed) in a 15 mL test tube. Cultures were incubated at 30 °C and 250 r.p.m. for 24 h. Experimental cultures (50 mL media in a 250 mL baffled shake flask) were inoculated from the pre-culture to at an initial OD_{600} of 0.2. Production cultures were incubated at 30°C and 250 r.p.m. for at least 96 hrs.

Sugarcane juice and oilcane hydrolysate were obtained from Dr. Vijay Singh of the Center for Advanced Bioenergy and Bioproducts Innovation and switchgrass hydrolysate was obtained from Great Lakes Bioenergy Research Center. After acquisition, sugar sources were sterilized using 0.22 μm filter and stored in -20°C prior to experimental use. Sugarcane juice media contains 90% v/v sugarcane juice and 100 mM phosphate buffer. The hydrolysate media contains 50% v/v oilcane/switchgrass hydrolysate, 10 g/L ammonium sulfate, 100 mM phosphate buffer, 1.7 g/L yeast nitrogen base w/o amino acids and ammonium sulfate and 0.77 g/L CSM. As described for defined media experiments, an overnight culture in YPD media was inoculated into 50 mL undefined media in a 250 mL baffled shake flask at an initial OD600 of 0.2-0.5. Production cultures were grown at 30°C and 250 r.p.m. for at least 96 hrs.

Bioreactor fermentations experiments were performed using the aforementioned defined media. The bioreactor seed train was produced as follows: a single colony was inoculated into 5 mL YPD media in a test tube, cultures were incubated at 30 °C and 250 r.p.m. overnight, and used to inoculate to 50 mL media in a shake flask at an initial OD_{600} of 0.2. Shake flask cultures were grown for 24 h at 30 °C and 250 r.p.m. The shake flask seed culture was used to inoculate to 0.5 L media in a bioreactor at an initial OD_{600} of 0.5. During fermentation, dissolved oxygen was maintained at 20% of maximum by varying rotor speed between 250 r.p.m and 1,000 r.p.m. with a constant air input flow rate of 2.0 L/min, pH was maintained at 5.5 or above with 2 M NaOH, and temperature was maintained at 30 °C. Samples (5-10 mL) were taken every 24 hrs, and

fermentation lasted 6-7 days. We ran multiple fermentations with suboptimal conditions before settling on the above parameters. Feeding solutions were prepared containing 500 g/L glucose, 0.1 M phosphate buffer, and 1.7 g/L yeast nitrogen base w/o amino acids and 32 g/L ammonium sulfate (maintain same C/N ratios as batch fermentation).

Quantification of sugar consumption

Glucose, sucrose, xylose, and fructose were quantified on an HPLC (Shimadzu) equipped with an autosampler, quaternary pump, degasser and a refractive index detector. 1 mL fermentation broth samples were prepared by centrifuging at 15,000× *g* and filtering the supernatant through a 0.22 µm membrane filter. For each sample, 10 µL was injected and separated for 25 min on a Restek Organic Acids column with a mobile phase of 5 mM H_2SO_4 at a flow rate of 0.6 mL/min. Standards (manufacturer) were run at the following concentrations to generate a peak area-based standard curve: 100, 50, 25, 10, 5, 1 g/L.

Confocal microscopy

To harvest, one OD-mL of culture was spun down at 1,000 × *g* for 3 min and resuspended in 500 µL phosphate-buffered Saline solution (PBS). In brief 6 µL of 1 mM nile red (dissolved in DMSO) was added and then cells were incubated in the dark at room temperature for 15 min. Cells were spun down at 1,000×*g* for 3 min, resuspended in 800 µL ice cold water, spun down again and resuspended again in 800 µL ice cold water. 2-5 µL stained cells were plated on slides and air dried fixed. Fixed cells were washed one time with 1 mL PBS. Cells were air dried on the slides and fixed with 4% PFA (Paraformaldehyde). After washed three times with PBS, cells were mounted with ProLong Gold antifade reagent (Invitrogen, Waltham, MA). Images were acquired on Nikon A1RS HD Confocal microscope (100 × oil objective).

Quantifications of dry cell weight and lipids

In general, lipid extraction followed the Folch protocol with minor modification[52]. Specifically, 0.5 mL cell cultures were spun down at 4,500 ×*g* for 5 min in glass tubes and cell pellets were resuspended in autoclaved milliQ H_2O. We repeated the centrifuge and wash steps and cell pellets were frozen at -80°C for at least 30 min prior to being lyophilized overnight using a Labconco lyophilizer (Kansas City, MO). Dry cell weight was calculated by dividing measured dry cell weight (e.g. weight of glass + cells – weight of glass alone, mg) over total cell volume (e.g. 0.5 mL). 1-5 mg dried cell pellets were used for lipid extraction. Next, 50 µL internal standards 2.5 mg/mL triheptadecanoin, 5 mL MeOH/chloroform (v/v 1:1) and ~500 µL glass beads were added into each tube and vortexed at 1,500 r.p.m. for 30 min. Then, 2.5 mL milliQ H_2O was added to each tube and samples were vortexed 2 min at 1,500 r.p.m. Samples were centrifuged at room temperature and 1,000 ×*g* for 10 min. Cell debris and aqueous phase were aspirated and chloroform layer was saved. Chloroform solvent was removed by evaporation using a Thermo Scientific speedvac (Waltham, MA) to leave lipid pellets at the bottom of the tube. For HPLC-MS analysis of intact acTAG, 500 µl MeOH were added to resuspend lipids. For quantification, acTAG were derivatized to fatty acyl methyl esters. 500 µl HCL-MeOH solution was added and the reaction was performed in a 50°C water bath for 12 hrs. Next, 1 mL hexane and 5 mL 100 mg/mL $NaHCO_3$ was added to terminate and neutralize each reaction. The samples were vortexed for 5 min at 1,500 r.p.m. and centrifuged at 1,000×*g* and room temperature for 10 min. The hexane layers were carefully collected and used for GC-FID analysis. Fatty acyl methyl esters were separated using an Agilent RTX-5 column and were quantified by comparing GC-FID peak areas against standard curves prepared with commercial standards[53,54].

LC-MS analysis was carried out on a Vanquish UPLC coupled by an electrospray ionization source operating in positive mode to a Q Exactive Orbitrap high-resolution mass spectrometer (ThermoScientific)[55]. Chromatographic separation of lipid samples resuspended in methanol

occurred on a 2.1x100 mm ACQUITY UHPLC CSH (charged surface hybrid) C18 column with 1.7 µm particle size (Waters) heated to 50°C. Solvent A was 70:30 acetonitrile:water with 10 mM ammonium acetate and 250 µL/L acetic acid; solvent B was 90:10 isopropanol:acetonitrile with 10 mM ammonium acetate and 250 µL/L acetic acid. A flow rate of 0.3 mL/min and the following gradient were used for separation: 0-2 min, 2% B; 2-5 min, linear gradient from 2 to 30% B; 5-22 min, linear gradient from 30 to 99% B; 22-29 min, 99% B; 29-30 min, linear gradient from 99 to 2% B; 30-35 min, 2% B.

The mass spectrometer was used to collect both full-MS and MS2 spectra using a data-dependent acquisition method (full MS-ddMS2). Full MS parameters were a scan range of 240-1,600 m/z, automatic control gain (ACG) target of 3 e^6, maximum injection time (IT) of 100ms, and a resolution of 70,000 full width at half maximum (FWHM). MS2 parameters were ACG target of 5 e^5, maximum IT of 80 ms, minimum ACG target of 8 e^3, isolation window of 1.4 m/z, resolution of 35,000 FWHM, loop count of 5, and stepped nominal collision energy (NCE) of 30, 40. Phosphatidylglycerol (PG, 16:0,16:0) was identified in the adduct form of $[M+NH_4]+$ at m/z 740.5436[55]. Each acTAG/lcTAG species was validated at the expected m/z of the parent [M+NH4]+ adduct. acTAG/PG or lcTAG/PG of peak area ratios were calculated to estimate the abundance of each lipid given the corresponding fatty acid content calculated from FAME analysis.

Techno-economic analysis

Two oilcane biorefinery configurations for the production of acTAG were developed in BioSTEAM[41,42]: (i) a conventional sugarcane biorefinery and (ii) a lignocellulosic switchgrass biorefinery using ammonia fiber expansion pretreatment (AFEX) (**Supplementary Fig. 16-19**). Based on data from the Center for Bioenergy and Bioproducts Innovation, 40% of the vegetable oil can remain in the bagasse after juicing and 70% of this oil can be extracted downstream after

pretreatment and hydrolysis. Therefore, the OJ configuration represents a low cost and low oil recovery installation compared to the OJH configuration. Given that no industrial production process for fermentation-derived acTAG currently exists, the biorefinery models developed in this study are preliminary designs for the conceptual production of acTAG. Both biorefineries produce acTAG, biodiesel, and excess electricity from burning biomass residue. The lipids are extracted by first centrifuging out the lipids in solution and the cell mass from the fermentation broth. Then, a drier reduces the cell mass moisture content to 18% and a screw press is used to extract 70% of the lipids contained in the cell mass[56]. The lipid is then washed and vacuum dried to remove any impurities. The dried lipid is dry fractionated following the design of conventional dry fractionation of olein and stearin from palm kernel oil, whereby the stearin is crystallized from the melt and separated by a membrane pressure filter[57] (**Supplementary Fig. 18**). The melt fraction containing 90% acTAG is sold. The solid fraction with polar lipids (PL), free fatty acids (FFA), acTAG, and lcTAG is remelted, pretreated, and transesterified to produce biodiesel[58]. General techno-economic parameters follow the assumptions by NREL's detailed design report for a corn stover biorefinery, including modeling of specialized equipment, capital cost correlations, prices, plant size, and operation[59]. The cellulase mixture is purchased at a concentration of 50 g/L and a price of 0.424 $/kg. The price of cellulase is the production cost for the on-site cellulase production process modeled by NREL[59]. Feedstock compositions are listed in **Supplementary Tables 4 and 5**. Detailed bioreactor design and specifications are listed in **Supplementary Tables 6 and 7.** Assumptions on the dry fractionation process are listed in **Supplementary Table 8.** Capital and operating costs are listed in **Supplementary Tables 9, 10, and 11**. Additional discussion and details on the production process and accessing the biorefinery models are available in **Supplementary Method 3.**

While no markets have yet been established for acTAG produced by fermentation, their low viscosity can enable their use as a drop-in replacement for diesel #4, which is used in low to medium speed diesel engines[12]. The average market price for diesel #4 between 2000–2004 is listed as $145–225 /ton by the U.S. Energy Information Administration[44] (assuming a density of 0.9 kg/L). Retail prices for diesel #4 after 2004 are withheld by the EIA to avoid disclosure of individual company data. Fermentation derived acTAGs may also potentially serve as a food grade emulsifier, as acetylated mono- and diglycerides (i.e. ACETEM) are widely used for that purpose[13]. A preliminary survey of current selling prices for acetic acid esters of mono and diglycerides shows a market price range of $1633–2268 /ton[43] (**Supplementary Method 3.4**). The plant capacity for acTAG production in this work (maximally 0.09 million ton/yr) is well within the reported U.S. demand for diesel #4 (~50.4 million ton/yr in 2017)[44] as well as for food emulsifiers (projected to be ~1.4 million ton/yr in 2028)[43].

Statistical analysis

Each experiment was conducted with independently a minimum of three biological replicates. All data represent the mean ± s.d. of biological replicates. Standard deviation and *P* value were obtained using Microsoft Excel version 365 Apps for enterprise. *P* values were analyzed based on student two-tailed t-test assuming unequal variances.

References

1. Liao, J. C., Mi, L., Pontrelli, S. & Luo, S. Fuelling the future: microbial engineering for the production of sustainable biofuels. *Nat. Rev. Microbiol.* **14**, 288–304 (2016).
2. Zhou, Y. J., Kerkhoven, E. J. & Nielsen, J. Barriers and opportunities in bio-based production of hydrocarbons. *Nat. Energy* **3**, 925–935 (2018).
3. Moore, R. H. *et al.* Biofuel blending reduces particle emissions from aircraft engines at cruise conditions. *Nature* **543**, 411–415 (2017).
4. Yan, Q. & Pfleger, B. F. Revisiting metabolic engineering strategies for microbial synthesis of oleochemicals. *Metab. Eng.* **58**, 35–46 (2020).
5. Qiao, K., Wasylenko, T. M., Zhou, K., Xu, P. & Stephanopoulos, G. Lipid production in Yarrowia lipolytica is maximized by engineering cytosolic redox metabolism. *Nat. Biotechnol.* **35**, 173–177 (2017).
6. Blazeck, J. *et al.* Harnessing Yarrowia lipolytica lipogenesis to create a platform for lipid and biofuel production. *Nat. Commun.* **5**, 3131 (2014).
7. Sreeharsha, R. V. & Mohan, S. V. Obscure yet Promising Oleaginous Yeasts for Fuel and Chemical Production. *Trends Biotechnol.* **38**, 873–887 (2020).
8. Spagnuolo, M., Yaguchi, A. & Blenner, M. Oleaginous yeast for biofuel and oleochemical production. *Curr. Opin. Biotechnol.* **57**, 73–81 (2019).
9. Adrio, J. L. Oleaginous yeasts: Promising platforms for the production of oleochemicals and biofuels. *Biotechnol. Bioeng.* **114**, 1915–1920 (2017).
10. Marshall, K. E. *et al.* Seasonal accumulation of acetylated triacylglycerols by a freeze-tolerant insect. *J. Exp. Biol.* **217**, 1580–1587 (2014).
11. Durrett, T. P. *et al.* A distinct DGAT with sn-3 acetyltransferase activity that synthesizes unusual, reduced-viscosity oils in Euonymus and transgenic seeds. *Proc. Natl. Acad. Sci.* **107**, 9464–9469 (2010).
12. Liu, J. *et al.* Metabolic engineering of oilseed crops to produce high levels of novel acetyl glyceride oils with reduced viscosity, freezing point and calorific value. *Plant Biotechnol. J.* **13**, 858–865 (2015).
13. Gaupp, R. & Adams, W. Acid Esters of Mono- and Diglycerides. in *Emulsifiers in Food Technology* 93–120 (John Wiley & Sons, Ltd, 2014). doi:10.1002/9781118921265.ch5
14. Sitepu, I. R. *et al.* An improved high-throughput Nile red fluorescence assay for estimating intracellular lipids in a variety of yeast species. *J. Microbiol. Methods* **91**, 321–328 (2012).
15. Sørensen, L. B. *et al.* The effect of salatrim, a low-calorie modified triacylglycerol, on appetite and energy intake. *Am. J. Clin. Nutr.* **87**, 1163–1169 (2008).
16. Yang, H. O. *et al.* Stimulatory Effects of Monoacetyldiglycerides on Hematopoiesis. *Biol. Pharm. Bull.* **27**, 1121–1125 (2004).
17. Milcamps, A. *et al.* Isolation of a Gene Encoding a 1,2-Diacylglycerol- sn -acetyl-CoA Acetyltransferase from Developing Seeds of Euonymus alatus. *J. Biol. Chem.* **280**, 5370–5377 (2005).
18. Bansal, S. & Durrett, T. P. Defining the extreme substrate specificity of Euonymus alatus diacylglycerol acetyltransferase, an unusual membrane-bound O-acyltransferase. *Biosci. Rep.* **36**, (2016).

19. Tran, T. N. T., Shelton, J., Brown, S. & Durrett, T. P. Membrane topology and identification of key residues of Ea DAcT, a plant MBOAT with unusual substrate specificity. *Plant J.* **92**, 82–94 (2017).

20. Olzmann, J. A. & Carvalho, P. Dynamics and functions of lipid droplets. *Nat. Rev. Mol. Cell Biol.* **20**, 137–155 (2019).

21. Yang, H., Galea, A., Sytnyk, V. & Crossley, M. Controlling the size of lipid droplets: lipid and protein factors. *Curr. Opin. Cell Biol.* **24**, 509–516 (2012).

22. Thiam, A. R., Farese Jr, R. V. & Walther, T. C. The biophysics and cell biology of lipid droplets. *Nat. Rev. Mol. Cell Biol.* **14**, 775–786 (2013).

23. Luo, Z. *et al.* Enhancing isoprenoid synthesis in Yarrowia lipolytica by expressing the isopentenol utilization pathway and modulating intracellular hydrophobicity. *Metab. Eng.* **61**, 344–351 (2020).

24. Ma, T. *et al.* Lipid engineering combined with systematic metabolic engineering of Saccharomyces cerevisiae for high-yield production of lycopene. *Metab. Eng.* **52**, 134–142 (2019).

25. Sadre, R. *et al.* Cytosolic lipid droplets as engineered organelles for production and accumulation of terpenoid biomaterials in leaves. *Nat. Commun.* **10**, 853 (2019).

26. Bansal, S. *et al.* Towards the synthetic design of camelina oil enriched in tailored acetyl-triacylglycerols with medium-chain fatty acids. *J. Exp. Bot.* **69**, 4395–4402 (2018).

27. Tran, T. N. T. *et al.* Metabolic engineering of Saccharomyces cerevisiae to produce a reduced viscosity oil from lignocellulose. *Biotechnol. Biofuels* **10**, 69 (2017).

28. Yu, T. *et al.* Reprogramming Yeast Metabolism from Alcoholic Fermentation to Lipogenesis. *Cell* **174**, 1549-1558.e14 (2018).

29. Zhu, Z. *et al.* Multidimensional engineering of Saccharomyces cerevisiae for efficient synthesis of medium-chain fatty acids. *Nat. Catal.* **3**, 64–74 (2020).

30. Gajdoš, P., Hambalko, J., Nicaud, J. & Čertík, M. Overexpression of diacylglycerol acetyltransferase from <scp> *Euonymus europaeus* </scp> in *Yarrowia lipolytica* leads to the production of single-cell oil enriched with 3-acetyl-1,2-diacylglycerols. *Yeast* **37**, 141–147 (2020).

31. Pomraning, K. R. *et al.* Comprehensive Metabolomic, Lipidomic and Microscopic Profiling of Yarrowia lipolytica during Lipid Accumulation Identifies Targets for Increased Lipogenesis. *PLoS One* **10**, e0123188 (2015).

32. Dulermo, T. & Nicaud, J.-M. Involvement of the G3P shuttle and β-oxidation pathway in the control of TAG synthesis and lipid accumulation in Yarrowia lipolytica. *Metab. Eng.* **13**, 482–491 (2011).

33. Gajdoš, P., Ledesma-Amaro, R., Nicaud, J.-M., Čertík, M. & Rossignol, T. Overexpression of diacylglycerol acyltransferase in Yarrowia lipolytica affects lipid body size, number and distribution. *FEMS Yeast Res.* **16**, fow062 (2016).

34. Beopoulos, A. *et al.* Identification and characterization of DGA2, an acyltransferase of the DGAT1 acyl-CoA:diacylglycerol acyltransferase family in the oleaginous yeast Yarrowia lipolytica. New insights into the storage lipid metabolism of oleaginous yeasts. *Appl. Microbiol. Biotechnol.* **93**, 1523–1537 (2012).

35. Athenstaedt, K. YALI0E32769g (DGA1) and YALI0E16797g (LRO1) encode major

triacylglycerol synthases of the oleaginous yeast Yarrowia lipolytica. *Biochim. Biophys. Acta - Mol. Cell Biol. Lipids* **1811**, 587–596 (2011).

36. Wang, L. *et al.* Structure and mechanism of human diacylglycerol O-acyltransferase 1. *Nature* **581**, 329–332 (2020).

37. Blazeck, J., Liu, L., Redden, H. & Alper, H. Tuning Gene Expression in Yarrowia lipolytica by a Hybrid Promoter Approach. *Appl. Environ. Microbiol.* **77**, 7905–7914 (2011).

38. Cheng, M.-H. *et al.* Conversion of High-Solids Hydrothermally Pretreated Bioenergy Sorghum to Lipids and Ethanol Using Yeast Cultures. *ACS Sustain. Chem. Eng.* **9**, 8515–8525 (2021).

39. Serate, J. *et al.* Controlling microbial contamination during hydrolysis of AFEX-pretreated corn stover and switchgrass: effects on hydrolysate composition, microbial response and fermentation. *Biotechnol. Biofuels* **8**, 180 (2015).

40. Konzock, O., Zaghen, S. & Norbeck, J. Tolerance of Yarrowia lipolytica to inhibitors commonly found in lignocellulosic hydrolysates. *BMC Microbiol.* **21**, 77 (2021).

41. Cortés-Peña, Y. Thermosteam: BioSTEAM's Premier Thermodynamic Engine. *J. Open Source Softw.* **5**, 2814 (2020).

42. Cortes-Peña, Y., Kumar, D., Singh, V. & Guest, J. S. BioSTEAM: A Fast and Flexible Platform for the Design, Simulation, and Techno-Economic Analysis of Biorefineries under Uncertainty. *ACS Sustain. Chem. Eng.* **8**, 3302–3310 (2020).

43. *Food Emulsifiers Market Size By product (Mono, Di-Glycerides & Derivatives, Lecithin, Stearoyl Lactylates, Sorbitan Esters), By Application (Bakery & Confectionery, Food & Nutrition, Beverages, Dairy & Frozen Desserts, Sauces & Dressings), Regional Outloo*.

44. *Prices of refiner No. 4 fuel sales to end users by Administration, U.S. Energy Information*.

45. Friedlander, J. *et al.* Engineering of a high lipid producing Yarrowia lipolytica strain. *Biotechnol. Biofuels* **9**, 77 (2016).

46. Rutter, C. D., Zhang, S. & Rao, C. V. Engineering Yarrowia lipolytica for production of medium-chain fatty acids. *Appl. Microbiol. Biotechnol.* **99**, 7359–7368 (2015).

47. Nicaud, J. M., Fournier, P., La Bonnardière, C., Chasles, M. & Gaillardin, C. Use of ars18 based vectors to increase protein production in Yarrowia lipolytica. *J. Biotechnol.* **19**, 259–270 (1991).

48. Sambrook, J. & Russell, D. *Molecular Cloning: a Laboratory Manual*. (Cold Spring Harbor Laboratory Press, 2001).

49. Schwartz, C., Shabbir-Hussain, M., Frogue, K., Blenner, M. & Wheeldon, I. Standardized Markerless Gene Integration for Pathway Engineering in Yarrowia lipolytica. *ACS Synth. Biol.* **6**, 402–409 (2017).

50. Holkenbrink, C. *et al.* EasyCloneYALI: CRISPR/Cas9-Based Synthetic Toolbox for Engineering of the Yeast Yarrowia lipolytica. *Biotechnol. J.* **13**, 1700543 (2018).

51. Labun, K., Montague, T. G., Gagnon, J. A., Thyme, S. B. & Valen, E. CHOPCHOP v2: a web tool for the next generation of CRISPR genome engineering. *Nucleic Acids Res.* **44**, W272–W276 (2016).

52. FOLCH, J., LEES, M. & SLOANE STANLEY, G. H. A simple method for the isolation and purification of total lipides from animal tissues. *J. Biol. Chem.* **226**, 497–509 (1957).

53. Yan, Q. *et al.* Metabolic engineering strategies to produce medium-chain oleochemicals via acyl-ACP:CoA transacylase activity. (2021). doi:10.1038/s41467-022-29218-3

54. Yan, Q. *et al.* Metabolic engineering of β-oxidation to leverage thioesterases for production of 2-heptanone, 2-nonanone and 2-undecanone. *Metab. Eng.* **61**, 335–343 (2020).

55. Hutchins, P. D., Russell, J. D. & Coon, J. J. LipiDex: An Integrated Software Package for High-Confidence Lipid Identification. *Cell Syst.* **6**, 621-625.e5 (2018).

56. Kim, J. *et al.* Methods of downstream processing for the production of biodiesel from microalgae. *Biotechnol. Adv.* **31**, 862–876 (2013).

57. Koay, G. F. L., Chuah, T.-G. & Choong, T. S. Y. Economic feasibility assessment of one and two stages dry fractionation of palm kernel oil. *Ind. Crops Prod.* **49**, 437–444 (2013).

58. Arora, A. & Singh, V. Biodiesel production from engineered sugarcane lipids under uncertain feedstock compositions: Process design and techno-economic analysis. *Appl. Energy* **280**, 115933 (2020).

59. Humbird, D. *et al. Process Design and Economics for Biochemical Conversion of Lignocellulosic Biomass to Ethanol: Dilute-Acid Pretreatment and Enzymatic Hydrolysis of Corn Stover*. (2011). doi:10.2172/1013269

Acknowledgements

We would like to thank Lance Rodenkirch and the University of Wisconsin Optical Imaging Core for the help with confocal image data collection. We would like to thank Professor Christopher Rao for providing the *Y. lipolytica* PO1f strain and integrative vector pHPH. We would like to thank Professor Edgar Cahoon for providing acetydiheptadecanoin as a chemical standard of acTAG and the pY5 plasmid. We also thank Dr. Ming-Hsun Cheng and Dr. Vijay Singh at the University of Illinois at Urbana-Champaign for providing sugarcane juice and oilcane hydrolysate. We also thank Professor Yongsu Jin provide us valuable advices on choosing xylose utilizing pathway in *Yarrowia lipolytica*.

This work was funded by the DOE Center for Advanced Bioenergy and Bioproducts Innovation, the Great Lakes Bioenergy Research Center, and the Center for Bioenergy Innovation (U.S. Department of Energy, Office of Science, Office of Biological and Environmental Research under Award Number DE-SC0018420, DE-SC0018409, DE-AC05-00OR22725, subcontract no. 4000158665, respectively). Any opinions, findings, and conclusions or recommendations expressed in this publication are those of the author(s) and do not necessarily reflect the views of the U.S. Department of Energy.

Author contributions

QY: Conceptualization, Investigation, Data curation, Writing - original draft, Writing - review & editing. TBJ and DA: Investigation, Writing - review & editing. WTC and FVG: Investigation, Writing - review & editing. ZY and EVS: Investigation, Writing - review & editing. YC, and JSG: Investigation Writing - review & editing. SH, SSB, JRV and REO: Investigation. BFP: Conceptualization, Writing - original draft, Writing - review & editing, Supervision, Funding acquisition.

Competing interest

Authors declare that they have no competing interests.

Data availability

All data needed to evaluate the conclusions in the paper are present in the paper and/or the Supplementary Materials or Source Data.

Code availability

All data needed to evaluate the conclusions in the paper are present in the paper and/or the Supplementary Materials or Source Data.

Figures and Tables

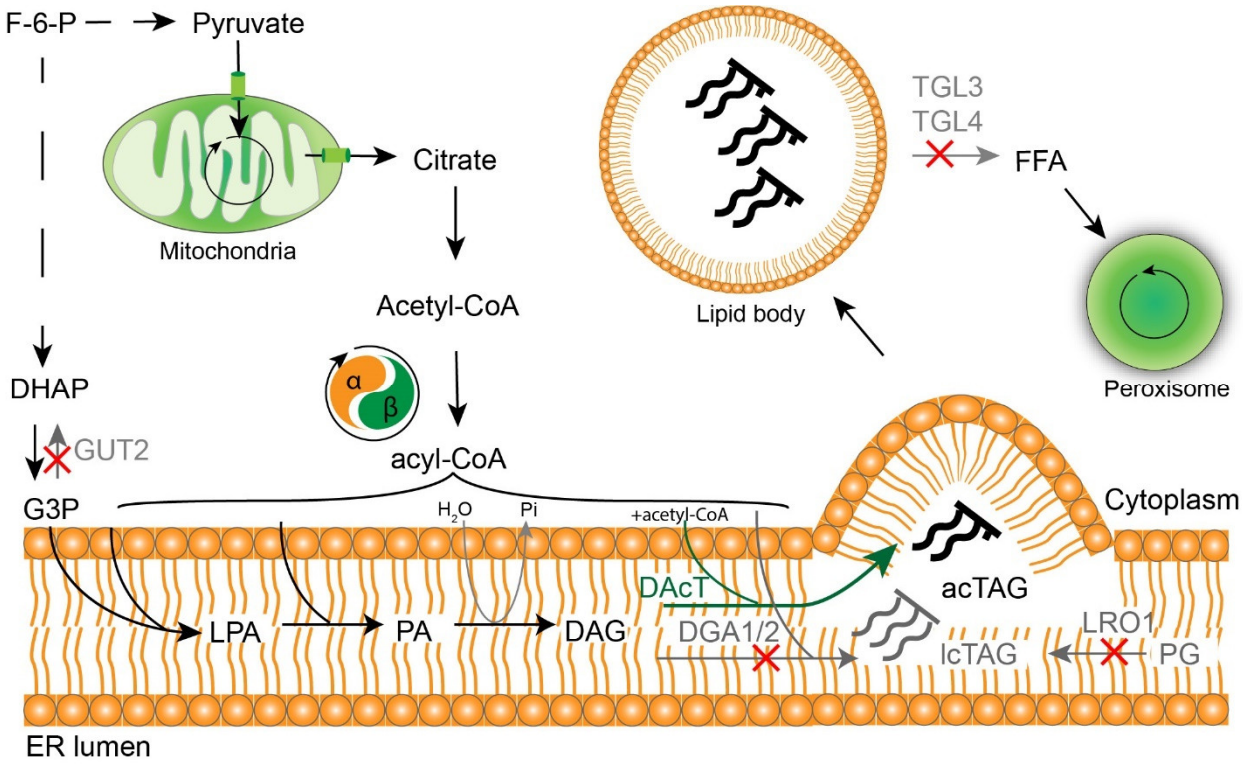

Fig. 1. Schematic of metabolic engineering strategies for acTAG production in *Y. lipolytica*. In yeast, the Kennedy pathway synthesizes long chain triacylglycerol (lcTAG) for incorporation into lipid bodies. Fatty acid biosynthesis generates long-chain acyl-CoAs that are transesterified with hydroxyl groups present in a glycerol moiety. The first transesterification takes place at the *sn*-1 position of glycerol-3-phosphate (G3P) to generate a lysophosphatidic acid (LPA). LPA undergoes a second transesterification at the *sn*-2 position, yielding a phosphatidic acid (PA) followed by a dephosphorylation at the *sn*-3 position to yield a diacylglycerol (DAG). DAG is the substrate for the final transesterification at the *sn*-3 position with either acyl-CoA, yielding a lcTAG, or acetyl-CoA, yielding an acTAG. As neutral lipids accumulate and coalesce within the ER bilayer, a lens-like structure forms ultimately leading to budding of a nascent lipid body into the cytoplasm. To enhance acTAG production, we deleted genes (symbolized by red cross) encoding enzymes that compete with acTAG flux. DGAT1, DGAT2, and LRO1 were deleted to prevent lcTAG formation. TGL3 and TGL4 were deleted to prevent consumption of neutral lipids. GUT2 was deleted to reduce G3P consumption. To produce acTAG, alternative synthases (DAcT) were heterologously expressed. Abbreviations: diacylglycerol (DAG), free fatty acid (FFA), glycerol-3-phosphate (G3P), lysophosphatidic acid (LPA), phosphatidylglycerol (PG), triacylglycerol lipase (TGL3 and TGL4), 1,2-diacylglycerol acyl-CoA transferase (DGA1 and DGA2), phospholipid acyl-CoA transferase (LRO1) glycerol-3-phosphate dehydrogenase (GUT2).

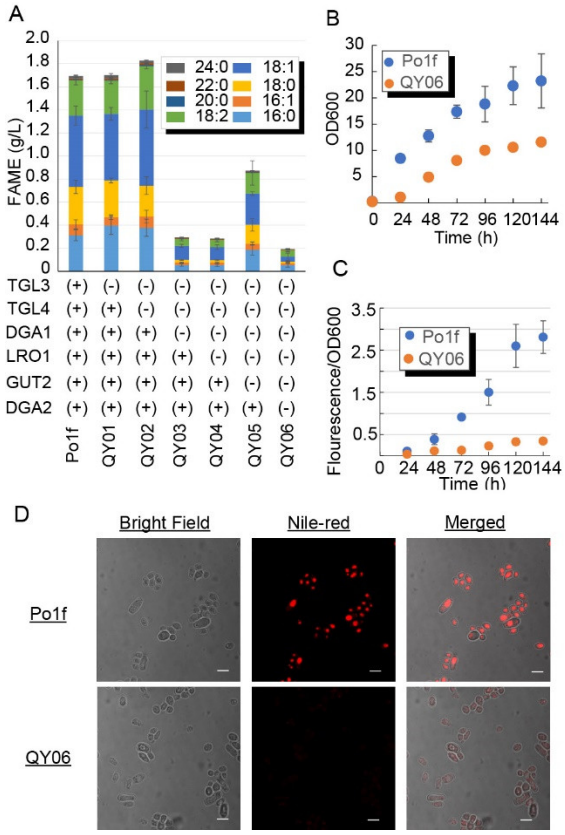

Fig. 2. Engineering strains to delete pathways that compete with acTAG flux. A) Titer of fatty acid methyl esters (FAME in g/L) derivatized from lipid extracts of cultures at 120 hrs. Deletions present in each strain are listed below the barchart, see **Fig. 1** for gene names. Acyl-chain lengths are sorted by color. B) Measurement of OD_{600} during cell growth at 24 hrs interval. C) Nile red fluorescence intensity/OD_{600} of stained cells sampled every 24 hrs. All data presented are the mean ± s.d. of biological replicates. (n=3 biologically independent samples) D) Confocal microscopic images of nile red stained cells at 120 hrs, 100× immersion oil. Cells were grown in YSC liquid media containing 80 g/L glucose at 30°C and 250 r.p.m. for 120 hrs.

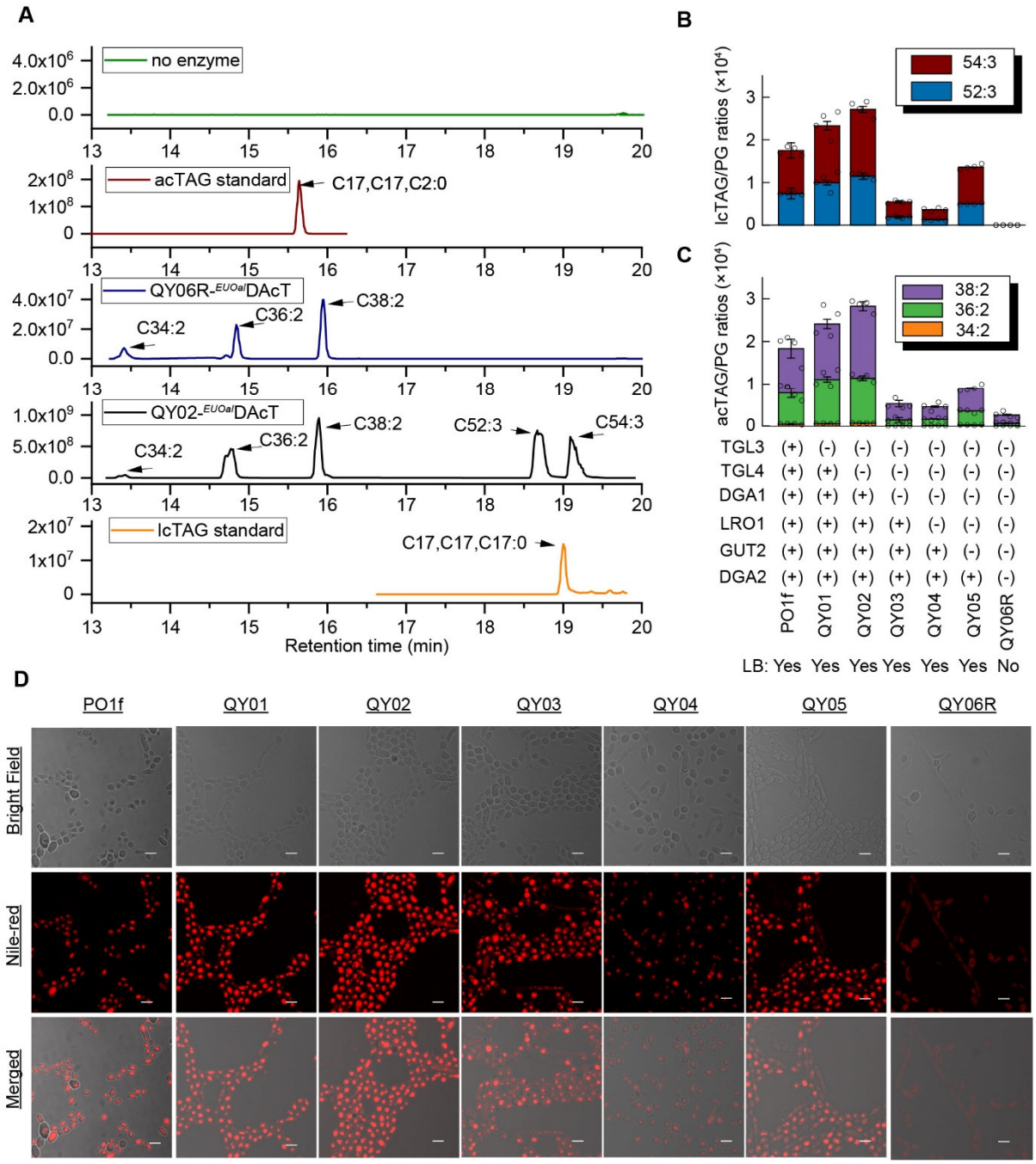

Fig. 3 Effect of the presence of lipid body on acTAG production. A) Extracted ion chromatogram of acTAGs and lcTAGs using HPLC-MS. 1,2-heptadecanoyl-3-acetyl triglyceride and lcTAG standard triheptadecanoin were used as external acTAG or lcTAG standard, respectively. acTAG molecules were identified in the adduct form of $[M+NH_4]+$ at m/z 624.52, 652.55 and 680.58 within a difference of 0.002 ppm. B) Quantification of ratios of lcTAG selected ion abundance to Phosphatidylglycerol (PG, 16:0,16:0) selected ion abundance is used to approximate relative lcTAG production per dry cell weight. C) Quantification of ratios of acTAG selected ion abundance to Phosphatidylglycerol (PG, 16:0,16:0) selected ion abundance to approximate relative acTAG production per dry cell weight. D) Confocal microscopic image of nile red stained cells at 120 hrs. Scale bar represented 10 μm. Cells PO1f, QY01-05 and QY06R harboring pY5-*EUOal*DAcT plasmid were grown in YSC-LEU liquid media containing 80 g/L glucose at 30°C and 250 r.p.m. for 120 hrs. All data presented are the mean ± s.d of biological replicates. (n=4 biologically independent samples).

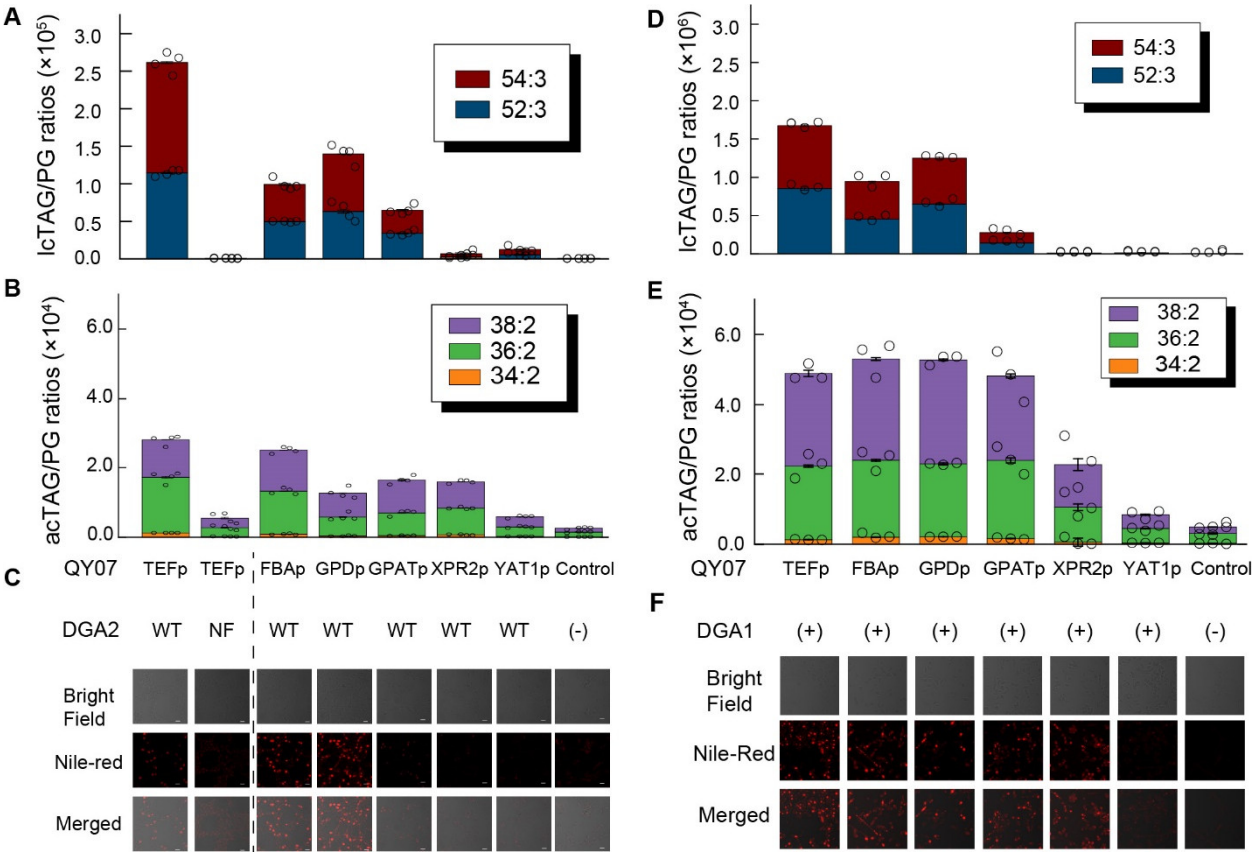

Fig. 4. **Effect of DGA1 and DGA2 functions on acTAG production.** A) lcTAG/PG ratios of selected ion abundances. B) acTAG/PG ratios of selected ion abundances. C) Confocal microscopic images of nile red stained cells at 120 hrs. Scale bar represents 10 µm. (n=4 biologically independent samples) D) lcTAG/PG ratios of selected ion abundances. E) acTAG/PG ratios of selected ion abundances. F) Confocal microscopic images of nile red stained cells at 120 hrs. Scale bar represents 10 µm. Cells were grown in YSC liquid media containing 80 g/L glucose, 0.1 M phosphate buffer and 300 mg/L Nat at 30 °C and 250 r.p.m. for 120 hrs (n=3 biologically independent samples). All data represent the mean ± s.d. of biological replicates. Control refers to a strain harboring an empty vector.

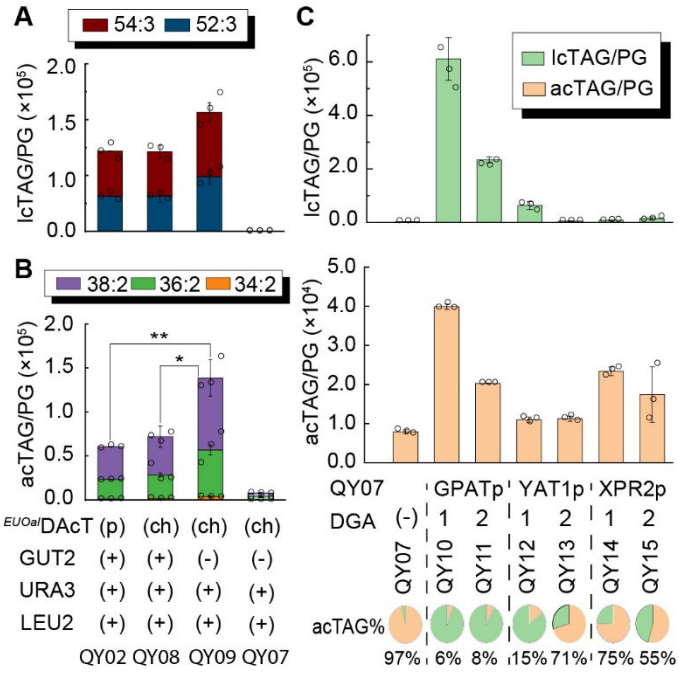

Fig. 5 Integrating metabolic engineering strategies to maximize acTAG production. A) lcTAG/PG ratios of selected ion abundances. B) acTAG/PG ratios of selected ion abundances. **P* = 0.01 and ***P* = 0.008 were analyzed based on student two-tailed t-test assuming unequal variances. (n=3 biologically independent samples) C) acTAG/PG and lcTAG/PG ratios of selected ion abundances (n=3 biologically independent samples). Cells were grown in YSC liquid media containing 80 g/L glucose and 0.1 M phosphate buffer at 30°C and 250 r.p.m. for 120 hrs. All data represent mean ± s.d. of biological replicates.

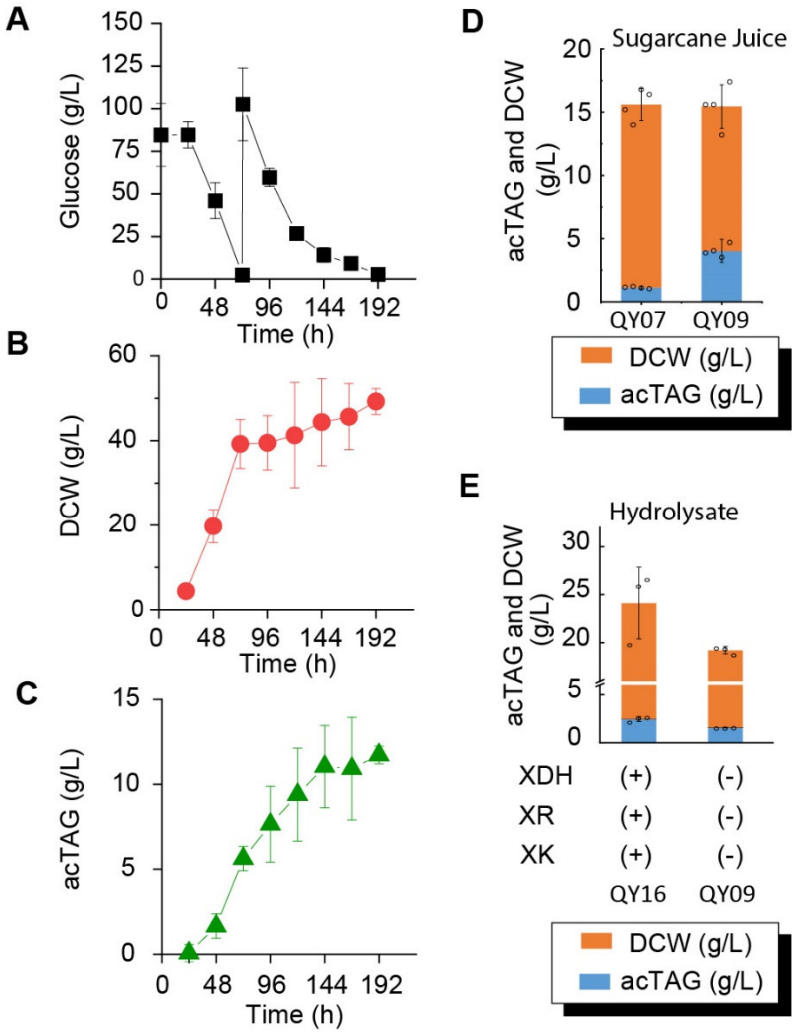

Fig. 6. Fed-batch fermentation for acTAG production Timecourse of (A) glucose consumption (g/L) biomass formation (dry cell weight g/L) and (C) acTAG volumetric titer (g/L) measured during a fed-batch culture of *Y. lipolytica* QY09. The acTAG titer (g/L) was calculated by multiplying the total measured FAME (g/L) by the fraction of acTAG selected ion abundance in acTAG + lcTAG selected ion abundance (e.g., 55%). The fed-batch was performed with YSC media containing 80 g/L glucose and 0.1 M phosphate buffer at 30°C, pH 5.5, and DO 20%. At the 72 hr mark, 100 g/L total glucose were bolus-fed to the media at 72 hrs. (D) acTAG (g/L) and cell biomass (DCW, g/L) produced from sugarcane juice (n=4 biologically independent samples). (E) acTAG (g/L) and cell biomass (DCW, g/L) produced from oilcane hydrolysate (n=3 biologically independent samples). Notably, the intracellular acTAG titer (g/L) from QY07 and QY09 were calculated by multiplying total FAME amount (g/L) and percentiles of acTAG selected ion abundance (e.g., 97% and 50%, respectively). Cells were grown in sugarcane juice liquid media or 50% (v/v) oilcane hydrolysate containing 0.1 M phosphate buffer at 30°C and 250 r.p.m. for 120 hrs. All data represent the mean ± s.d. of biological triplicates.

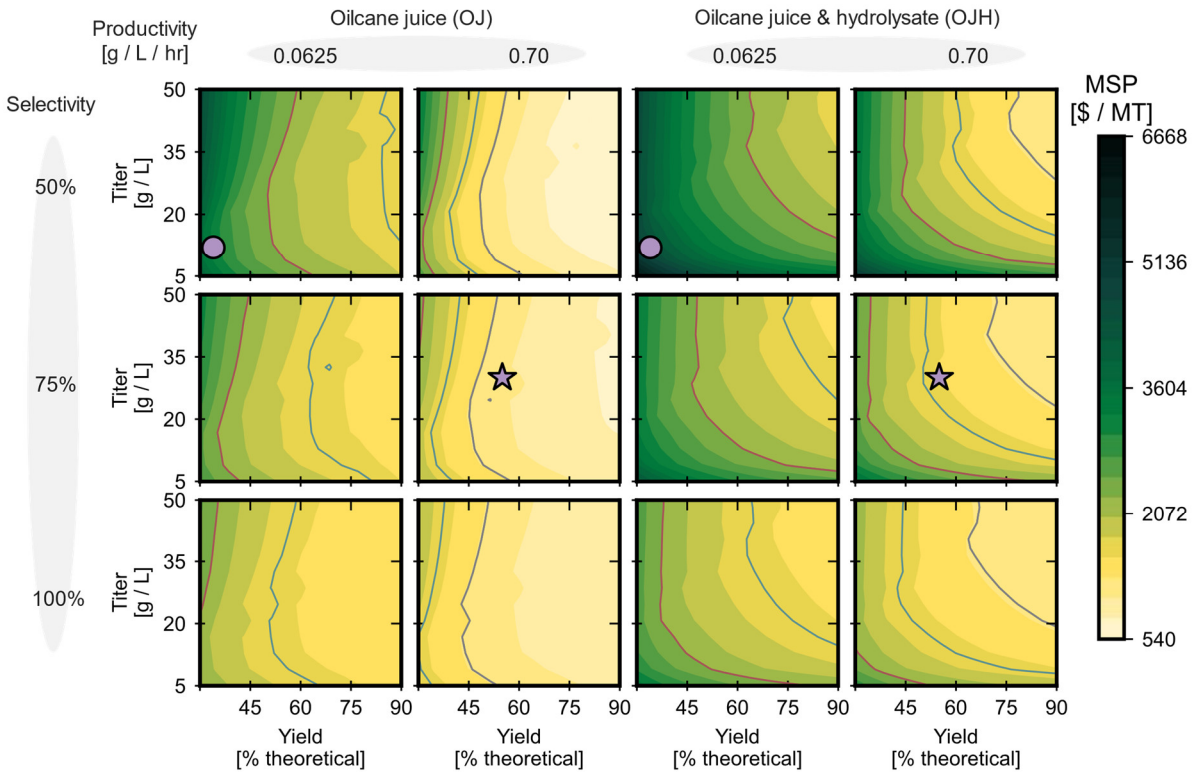

Fig. 7. Contours plot of the MSP of acTAG across yield in % theoretical of glucose consumption and titer in g/L for selectivity of 50, 75, and 100% acTAG (top, middle, and bottom rows; respectively) and productivities of 0.0625 and 0.7 g/L/h for both the OJ and the OJF biorefineries (left two and right two columns; respectively). The red and blue contours represent the lower and upper bounds of the market price food-grade emulsifiers ($1,633–2,268 /ton). The grey contour represents the price of biodiesel. The purple circles represent the baseline scenario (conservative assumptions on fermentation performance; 34% theoretical yield, 12 g/L titer, 50% acTAG selectivity, and 0.0625 g/L/h productivity), and the stars represent a potential target scenario (industrially relevant assumptions on fermentation performance; 30 g/L, 75 % acTAG selectivity, 55% theoretical yield, 0.7 g/L/h productivity).